Research Article | Vol. 9, No. 11 | 1 Nov 2018 | BIOMEDICAL OPTICS EXPRESS 5667
Biomedical Optics EXPRESS

# Noninvasive label-free detection of circulating white and red blood clots in deep vessels with a focused photoacoustic probe

**Mazen A. Juratli,[1,7] Yulian A. Menyaev,[2] Mustafa Sarimollaoglu,[2] Alexander V. Melerzanov,[3] Dmitry A. Nedosekin,[1] William C. Culp,[4] James Y. Suen,[5] Ekaterina I. Galanzha,[2,6] and Vladimir P. Zharov[2,6,8]**

[1]*Department of General and Visceral Surgery, University Hospital Frankfurt, Goethe-University, Frankfurt am Main, 60323, Germany*
[2]*Arkansas Nanomedicine Center, University of Arkansas for Medical Sciences, 4301 W. Markham St., Little Rock, AR 72205, USA*
[3]*Moscow Institute of Physics and Technology (MIPT), Moscow Region 141700, Russia*
[4]*Department of Radiology, University of Arkansas for Medical Sciences, 4301 W. Markham St., Little Rock, AR 72205, USA*
[5]*Department of Otolaryngology, Head and Neck Surgery, University of Arkansas for Medical Sciences, 4301 W. Markham St., Little Rock, AR 72205, USA*
[6]*Laboratory of Biomedical Photoacoustics, Saratov State University, 83, Astrakhanskaya St., Saratov, 410012, Russia*
[7]*mazen.juratli@kgu.de*
[8]*zharovvladimirp@uams.edu*

**Abstract**: Blood clotting is a serious clinical complication of many medical procedures and disorders including surgery, catheterization, transplantation, extracorporeal circuits, infections, and cancer. This complication leads to high patient morbidity and mortality due to clot-induced pulmonary embolism, stroke, and in some cases heart attack. Despite the clear medical significance, little progress has been made in developing the methods for detection of circulating blood clots (CBCs), also called emboli. We recently demonstrated the application of *in vivo* photoacoustic (PA) flow cytometry (PAFC) with unfocused ultrasound transducers for detection of CBCs in small vessels in a mouse model. In the current study, we extend applicability of PAFC for detection of CBCs in relatively large (1.5-2 mm) and deep (up to 5-6 mm) blood vessels in rat and rabbit models using a high pulse rate 1064 nm laser and focused ultrasound transducer with a central hole for an optic fiber. Employing phantoms and chemical activation of clotting, we demonstrated PA identification of white, red, and mixed CBCs producing negative, positive, and mixed PA contrast in blood background, respectively. We confirmed that PAFC can detect both red and white CBCs induced by microsurgical procedures, such as a needle or catheter insertion, as well as stroke modeled by injection of artificial clots. Our results show great potential for a PAFC diagnostic platform with a wearable PA fiber probe for diagnosis of thrombosis and embolism *in vivo* that is impossible with existing techniques.



## 1. Introduction

The genesis of circulating blood clot (CBC) formation called also emboli usually starts as a response to a blood vessel injury. Even in the absence of injury, many diseases and medical procedures may provoke the formation of CBCs that eventually block vessels at different locations [1–9]. Every year in the United States, over 795,000 individuals have a new or recurrent stroke often as a result of non-valvular atrial fibrillation, carotid disease, left ventricular dysfunction, or prosthetic valves. Pulmonary embolism (PE), the third most

#328947 https://doi.org/10.1364/BOE.9.005667
Journal © 2018 Received 25 Apr 2018; revised 24 Sep 2018; accepted 4 Oct 2018; published 23 Oct 2018

Biomedical Optics EXPRESS

common cause of hospital-related deaths, occurs as a result of a blood clot from a lower-extremity thromboembolism getting wedged into an artery in the lungs. Thus, thromboembolism (TE) typically occurs in the veins of the extremities, lungs (PE), brain (ischemic stroke), heart (myocardial infarction), kidney (acute renal failure), and the gastrointestinal tract [10–12]. TE is also a common complication of infection, inflammation, catheters, transplantation, extracorporeal circuits and surgery, including carotid endarterectomy and coronary artery bypass grafting [12–14].

Thrombotic events are also the second leading cause of death in cancer patients [15–19]. During the postoperative period, cancer patients showed a three-fold increase in venous thromboembolism (VTE) as compared with non-cancer patients, with at least 50% prevalence of postoperative thrombosis in the absence of proper prophylaxis.

Due to the lack of *in vivo* CBC detection methods, many CBCs remain undetectable, unless they result in a clinical phenomenon [20–21]. A significant number of patients die because of a failure in diagnosis rather than inadequate therapy. Additionally, no real-time monitoring of response to therapy has been developed that would allow an individualized treatment strategy. Existing diagnostic techniques *in vivo* can only detect static or slowly moving CBCs [22,23]. Fluorescence techniques can distinguish CBCs in blood microvessels (30–50 μm) in the animal model, but its translation to use in humans is problematic due to the cytotoxicity of fluorescent tags, difficulties with direct labeling of CBCs in the bloodstream, and the ability to only superficially assess microvessels with slow flow rates due to the strong autofluorescent background.

In a previous study, we demonstrated that *in vivo* PAFC can detect CBCs triggered by melanoma and microsurgical invasion. This study was focused on detection of CBCs in small (30-50 μm) peripheral blood vessels in a thin mouse ear [5,24].

In this article, we describe an advanced PAFC schematic using the customized focused ultrasound transducer for detection of CBCs in relatively deep (up to 5-6 mm) and large (up to 2 mm) vessels in rat and rabbit models. The obtained results demonstrate the translational potential of a PAFC diagnostic platform to be used in clinics to prevent PE and some strokes by early detection of CBCs followed by well-timed therapy.

## 2. Materials and methods

### *2.1 Principles of in vivo acoustic resolution PAFC platform*

The underlying principle of *in vivo* PAFC is described elsewhere [24–32]. Briefly, the use of short laser pulses to irradiate selected vessels containing circulating absorbing objects leads to the generation of acoustic waves (referred to as PA signals) which are detected in a time-resolved mode with an ultrasound transducer attached to the skin (Fig. 1(a)). The physical mechanism of PAFC is based upon the PA effect associated with fast (picosecond scale) non-irradiating relaxation of absorbed laser energy into heat and then the thermoelastic generation of acoustic waves. PAFC, as a combination of laser and ultrasound techniques, has the high sensitivity and spectral specificity of optical methods along with the high spatial resolution and the high depth penetration of ultrasound methods.

Laser irradiation of blood vessels creates a constant PA background determined by the absorption of many red blood cells (RBCs) randomly distributed in the irradiated detection volume [33–35]. Depending on the size of the vessels, hematocrit (Ht), as well as PAFC spatial resolution, the number of RBCs in the detected volume could vary, from one or a few RBCs in the capillary to thousands in larger vessels. When an RBC-rich red CBC passes through the irradiated blood volume, a transient increase in the local absorption, which is associated with a high concentration of hemoglobin (Hb), results in a sharp positive PA peak. Red Hb-rich CBCs can be detected when they have a higher local absorption than the normal RBC background in the detected volume. When weakly absorbing platelet-rich and/or fibrin-rich and/or white blood cell (WBCs)-rich white CBCs pass through the laser-irradiated vessel volume, a transient decrease in the local absorption results in a sharp negative PA signal.

Biomedical Optics EXPRESS

Finally, in case of mixed red-white CBCs, patterns of positive and negative PA signals are produced (Fig. 1(b)).

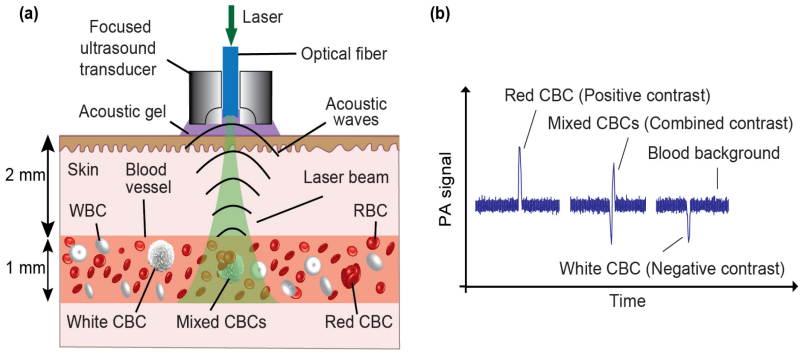


Fig. 1. The principle of PA detection of red, white and mixed CBCs producing positive, negative and combined PA contrast peaks in blood background, respectively. (a) Schematic of acoustic resolution PAFC diagnostic platform using a high pulse-repetition-rate laser and focused ultrasound transducer with a central hole to deliver laser light through a fiber. (b) PA trace showing PA peaks with positive (red CBC), negative (white CBC) and combined (mixed CBCs) contrast in the blood background.

Negative contrast depends on the absorption of the CBCs and the blood background, the vessel size, and the transducer acoustic resolution. In small vessels, blood background fluctuation is determined by random changes in the number of RBCs in the detection volume. In larger vessels containing hundreds or thousands of RBCs in the detection volume, RBCs-related fluctuations are minimized. The instability of the PA baseline is determined by laser pulse energy fluctuation (typically ≤ 2-4%), electrical and acoustic noise, vibration, and physiological rhythms (e.g., heartbeat or breathing). The duration of the transient PA signals, both positive and negative, is short (~$10^{-3}$ s), while the motion and other artifacts lies in the longer period of time >0.01s [5,24,32]. In the current study we have used a laser with relatively low energy fluctuation (<3%). Other sources produced relatively slow baseline fluctuation (time scale >10 ms) compared to a signal duration (0.1-2 ms), which allowed their effective filtration in the current work and as described in our recent paper [32]. All *in vivo* experiments were performed by delivery of laser light to the skin through an optical fiber in the central hole of a focused ultrasound transducer. Because of low optical resolution (OR) in deep tissue, we used the acoustic resolution (AR) PA probe, in which the lateral AR at the depth of 6-8 mm was estimated down to 45 µm.

### *2.2 PAFC setup*

The ytterbium fiber laser YLPM-0.3-A1-60-18 (IPG Photonics Corp.) emitted 1064 nm wavelength pulses with a pulse repetition rate of 10 kHz and pulse width of 10 ns. Maximum pulse energy measured at a distal optical tip was 240 µJ, although we reduced this level by orders of magnitude due to the high sensitivity of PAFC. A red pilot laser CPS180 (Thorlabs, Inc.) with 635 nm wavelength was used to navigate the 1064 nm laser beam. The laser beam spot was produced by a 330-µm optical fiber (CeramOptec Industries, Inc.) mounted inside a customized focused transducer. Therefore, both lasers were initially adjusted to the same pathway by using a dichroic mirror.

Laser power and pulse energy were monitored by USB meter PM100USB with head S302C (Thorlabs, Inc.). PAFC data acquisition was performed using the digitizer ATS9350 (Alazar Technologies, Inc.). Related software to record and process the data was developed in MATLAB (MathWorks, Inc.). Synchronization of laser pulses with data acquisition is provided by a 150 MHz bandwidth photodetector (PDA10A, Thorlabs, Inc.).

Biomedical Optics EXPRESS

### 2.3 Animal models

All protocols of animal-related experiments were approved by the University of Arkansas for Medical Sciences, Institutional Animal Care and Use Committee. The *in vivo* capabilities of the PA probe were tested in a rat model involving the carotid artery with a diameter of ~2 mm at a depth of 3–4 mm, and the tail vein with a diameter of ~0.5 mm at a depth of 0.3 mm. We also used a rabbit model involving an ear vein with a diameter of 0.6 mm at a depth of 0.5-1 mm, and the femoral vein with a diameter of 1–2 mm at a depth of 4.5–5 mm (Table 1). The transducer was placed above the skin at a point of vessel detection and were adjusted in real-time by maximizing PA signal amplitudes (Fig. 2(a)-2(d)). Ultrasound gel (Aquasonic Clear, Parker Labs, Inc.) was used for acoustic coupling between transducer and skin. Ultrasound images of the analyzed vessels were periodically acquired with a medical ultrasound system (M7, Mindray DS, Inc.).

**Table 1. The parameters of blood vessels tested with PAFC**

| Animal | Vessel | Diameter (mm) | Depth (mm) |
|---|---|---|---|
| Rat | Carotid artery | 2 | 3-4 |
| | Tail vein | 0.5 | 0.3 |
| Rabbit | Ear vein | 0.6 | 0.5-1 |
| | Femoral vein | 1-2 | 4.5-5 |

In the rat model, Sprague-Dawley rats were anesthetized by isoflurane inhalation (1.5%) and placed on a temperature-controlled stage (37°C). First, to determine the effects of needle injury on CBC dynamic, we inserted a 20-gauge needle into a rat tail vein and later into the left side of the heart and monitored the same vein at a distance of ~1 cm from the injection site tail vein or the carotid artery, respectively. To model white CBCs, injections of a single 100-μm-diameter transparent (i.e., low light absorbing) glass beads (Bio Spec Products, Inc.) mixed in 1 mL of phosphate buffered saline (PBS) (Sigma-Aldrich, Inc.) were administered into the rat's tail vein and into the rat heart (intracardiac). Noninvasive monitoring of PA signals occurred at the same tail vein at a distance of ~1 cm from the injection site, and in the carotid artery, at a distance of ~1 cm from the heart, after the intracardiac injection. We also used well-established chemicals to activate the formation of clots [4–6]. Specifically, the PA probe monitored the blood response in the carotid artery. After 30 minutes of continuous PA monitoring of the blood background, we injected collagen (0.2 mg/kg, Chrono-log-Corp.) into the heart of a rat, which simulated leukocyte/platelet-rich (white) clot formation. Later, Dextran 500, an activator of RBC aggregation (red CBCs), was injected into the heart of a rat after disappearance of the PA signals caused by collagen injection, and return of PA signals to the blood background level. Each rat was monitored using the PAFC for approximately 3 hours.

Biomedical Optics EXPRESS

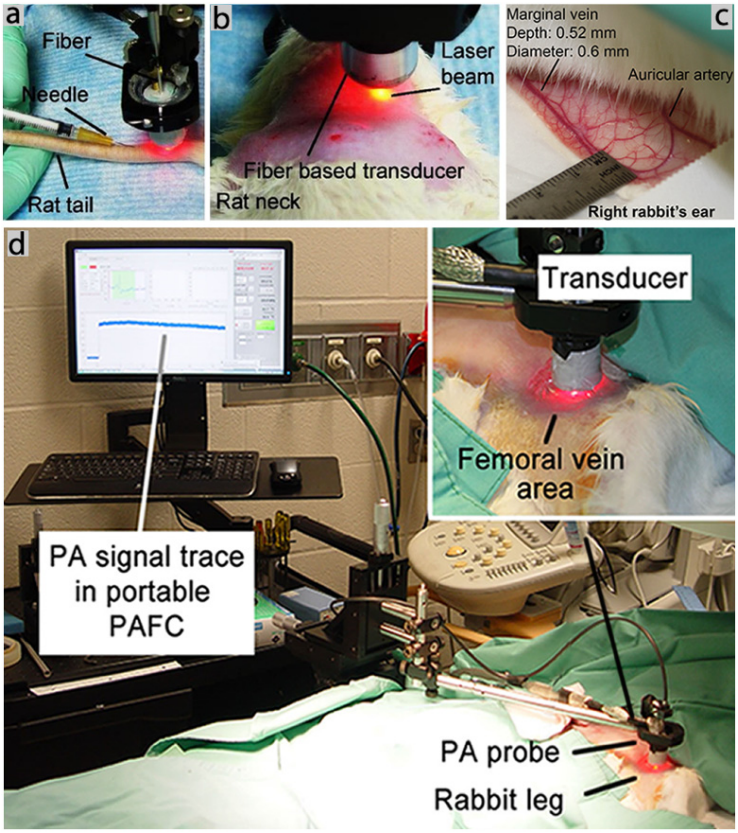


Fig. 2. Photos of animal model fragments and experimental schematics. (a) Picture of a rat tail during needle insertion. The PA probe was located on the same tail vein. (b) Picture of a rat neck after shaving the skin. The PA probe was located on the carotid artery. (c) Picture of the rabbit's right ear. (d) Pictures of the *in vivo* PAFC setup in a rabbit model. The PA probe was located on the femoral vein after shaving the skin.

In the rabbit model, a New Zealand White rabbit (the weight of 5.1 kg) was sedated with intramuscular ketamine (30mg/kg; Ketaset, Fort Dodge Animal Health, Inc.) and xylazine (3mg/kg, AnaSed, Lloyd Laboratories, Inc.) and maintained under anesthesia by mask ventilation with 1–1.5% isoflurane (Novaplus; Hospira-Inc.). To verify the PA probe's performance in large and deep vessels, real-time in vivo PAFC monitoring of microbubbles and CBCs phantoms in blood flow was performed on an ear vein and on a shaved inguinal area above the femoral vein. For this purpose, 3-French catheter (1 mm in diameter) was inserted inside the femoral artery and moved to the internal carotid artery. Then, a suspension of 900-µm-diameter spheres in 3 mL of PBS as large-clot phantoms was injected to produce stroke in the rabbit model. We also injected the perflutren lipid microbubbles (an ultrasound contrast agent) with an average of 2-3-µm-diameter and a small percentage at 10-20-µm-diameter (Definity; Lantheus Medical Imaging). During these procedures, the PA probe was placed on the rabbit's ear above vein or on skin above the femoral vein.

### *2.4 Data processing*

All the measurements were performed at least three times. The PA signals were acquired and points at least 3-sigma above the blood background were considered. PA signal rate is described as a number of signals per minute. Collected data ($M$ counts) are presented as $M \pm SD$. Signal and statistical analysis were utilized with a help of MATLAB (MathWorks, Inc.) software.

Biomedical Optics EXPRESS

## 3. Results

### *3.1 Specificity and sensitivity*

To determine the sensitivity of the *in vivo* PAFC technique, three rats in the control group were monitored for over 30 minutes, for which the PA probe was placed on the carotid artery. As a result of this procedure, no PA signals were observed (i.e., no false-positivity). To verify these data, the rats were monitored additionally at the area of carotid artery for next 30 min again, and no false-positive signals were acquired either (Fig. 3(a)).

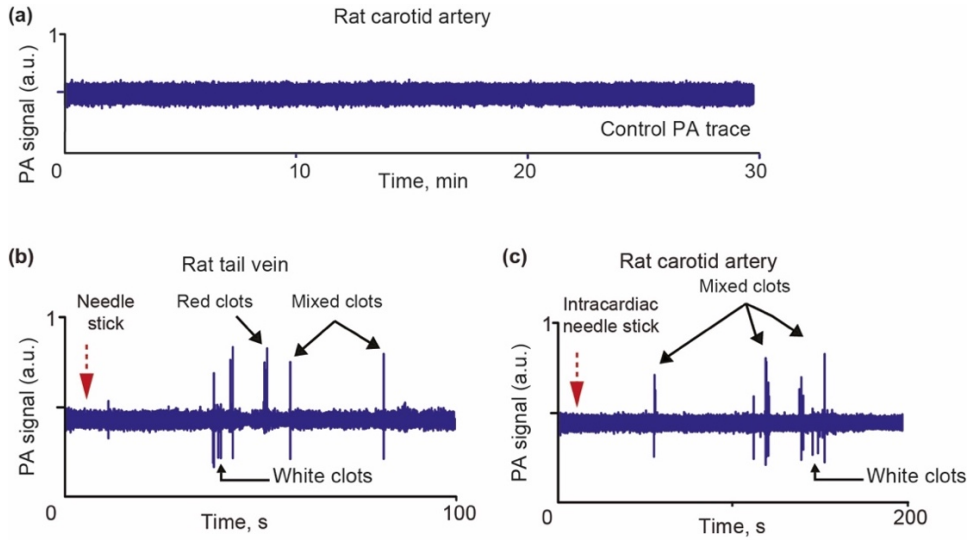


Fig. 3. (a) Example of PA trace from a carotid artery of rat in control group. Example of formation of red, white and mixed CBCs after vessel wall damage through needle insertion in tail vein (b) and carotid artery (c).

### *3.2 Correlation between vessel wall damage through needle insertion and CBC formation*

To determine the effect of needle insertion on the CBC dynamic, a 20-gauge needle was inserted into a tail vein, and later into the heart of a rat. The PA probe was placed on skin above the tail vein and the carotid artery, respectively. Around 1 minute after needle insertion, red, white and mixed CBCs were observed during 2 minutes of monitoring (Fig. 3(b), 3(c)).

### *3.3 Intravenous and intracardiac injection of collagen and Dextran 500*

After 30 minutes of continuous PA monitoring of the blood background in the carotid artery, collagen was injected directly into the rat's heart. One minute later, we observed the appearance of an average of 69 ± 15 mimic white CBCs per 30 minutes (Fig. 4(a)). After disappearance of the PA signals from mimic white CBCs (~90 min after injection), we injected Dextran 500 into the heart of the rat. In this case, we observed an average of 19 ± 6 mimic red CBCs per 30 minutes (Fig. 4(b)). The rate of PA signal appearance gradually decreased over 1 hour.

In particular, the PA amplitude distributions (mean ± SD) for positive peaks (typical for dextran injection) was 110.87 ± 30.59 (28%), 95.64 ± 36.34 (38%) and 79.18 ± 32.60 (41%), while the PA amplitude distributions for negative peaks (typical for collagen injection) was 91.08 ± 18.58 (20%), 107.46 ± 29.95 (28%), and 84.44 ± 36.52 (43%) (Fig. 4(c)).

Biomedical Optics EXPRESS

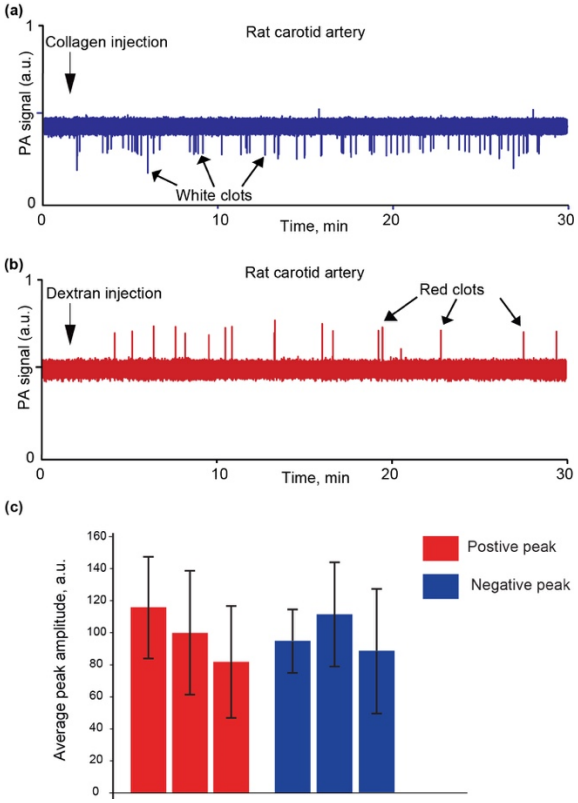


Fig. 4. Examples of PA traces from the vessels in rats after collagen (a) and Dextran 500 (b) injection. (c) Comparison of PA peak amplitude fluctuations of positive (red) and negative (blue) contrast for three rats.

### *3.4 Injection of a single 100-µm-diameter low-absorbing glass bead*

To demonstrate the ability of the focused PA probe to detect a single white CBC both in superficial and deep vessels, single 100-µm-diameter low-absorbing glass beads were repeatedly injected. On average, 1–2 seconds after each single-bead injection into the rat's tail vein, a PA negative-contrast signal corresponding to the passage of this bead through the laser beam was observed in the same vein at a distance of approximately 1 cm from the injection site (Fig. 5(a)). Similar results were obtained by single-bead injections into the rat's heart and noninvasive monitoring of PA signals in the carotid artery (Fig. 5(b)).

### *3.5 Injection of 900-µm-diameter spheres and gas-filled microbubbles*

A few white CBCs appeared 10-15 seconds after the PA probe was placed on the rabbit ear vein and a 3-French catheter (1 mm in diameter) was inserted inside the right femoral artery (Fig. (5c)). We also noninvasively monitored the rabbit ear vessels and a femoral vein during a stroke (confirmed by CT and ultrasound imaging), modeled by injection of artificial clots such as 0.9-mm-diameter beads through a catheter into the internal carotid artery. During this study, we observed both red and white CBCs in rabbit ear vessel. Specifically, a positive peak associated with red CBC was first observed (Fig. 5(d)). This appeared likely after the catheter insertion. Then, negative peak associated with white CBC was noticed after mimic clot injection. It was likely related to stroke-induced vessel injury, which can cause CBCs. Injection through a catheter of perflutren lipid microbubbles (an ultrasound contrast agent) led to the appearance of a few negative PA peaks (Fig. 5(e)), confirming PAFC's capacity to detect small circulating microbubbles.

Biomedical Optics EXPRESS

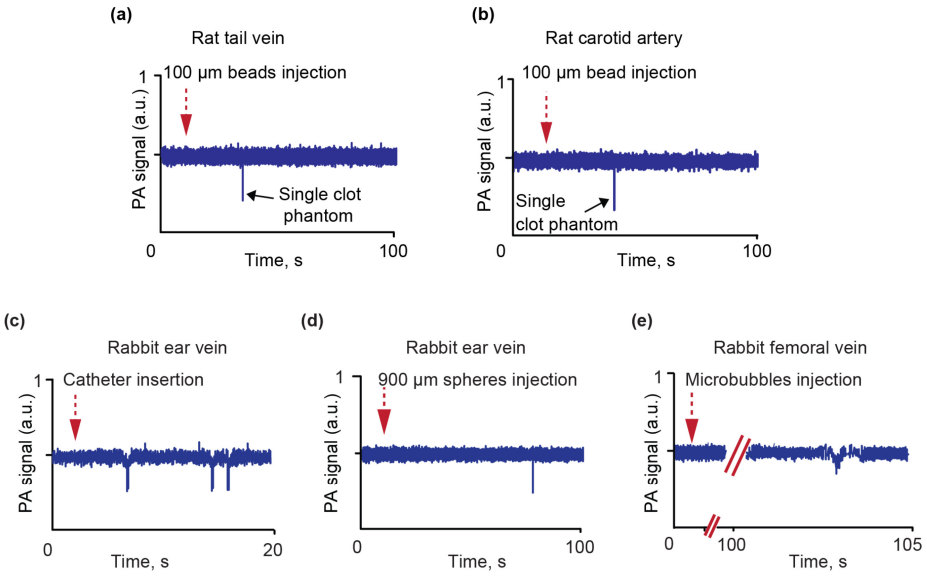


Fig. 5. Examples of PA traces in the rat model after transparent bead injection in rat tail vein and PA monitoring in tail vein (a) and carotid artery (b). Examples of PA traces in the rabbit model after catheter insertion (c), injection of transparent spheres (d) and microbubbles injections (e).

## 4. Discussion

In a previous study, we introduced a new diagnostic technique - *in vivo* PAFC platform for detection of circulating tumor cells (CTCs) (e.g., in melanoma patients), infections (e.g., malaria) and CBCs [24,25,28–30,32–34]. These pioneer results, however, were only demonstrated for small (30-50 µm) superficial vessels in small animal models (mice). In the present study, using new PA fiber-based probe with the focused transducer, we significantly extended application of PAFC platform on the analysis of CBCs in relatively large (1.5-2 mm) and deep (up to 5-6 mm) vessels in larger animal models (rat and rabbit). Moreover, based on the identification of negative, positive, and combined PA contrast in the blood background, we were able to monitor white, red, and mixed (white-red) CBCs, respectively.

The high sensitivity *in vivo* PAFC for detection of CBCs in deep and large vessels was confirmed by monitoring the carotid artery in a rat through injection of chemicals in the blood network. Specifically, collagen, which simulates leukocyte/platelet-rich (white) CBC formation, and Dextran 500, which is an activator of RBC aggregation (red CBCs clots), were injected into the rat heart. As expected, negative peaks associated with white CBCs appeared after injection of collagen, and positive peaks associated with red CBCs were observed after injection of Dextran 500. In both cases, the PA probe was located on skin above the carotid artery. The presented data (e.g., in Fig. 4) are indicative for a relatively good PA signal amplitude's consistency, taking into account it dependence on the reproducibility of the animal physiological parameters and the injection procedure consistency – in addition its dependency on PAFC device reproducibility. For comparison, according to our recent data obtained with a stable vessel phantom (i.e. no influence of the animal and injection parameters) the reproducibility of the PAFC device itself was found at a level of 14.8% [35].

After we confirmed proof of the concept, we inserted a catheter inside large vessels. The goal of this procedure was to understand the physiological vessels response on injury and vessel wall damage. We observed *in vivo* that the vessels, blood and immune systems respond through appearance of red CBCs as reaction to repair the wall damage, white CBCs appear as reaction to inflammation, and combined red and white CBCs to both processes. We also

Biomedical Optics EXPRESS

demonstrated the ability of the *in vivo* PAFC with a focused ultrasound probe to detect single white CBC after injection of single 100-µm-diameter low-absorbing glass beads as well as 900-µm-diameter transparent spheres in the stroke rabbit model.

The major challenge for PAFC is to detect the rare circulating objects in large blood vessels to ensure screening of significant blood volumes. This goal dictates that PAFC design should have a wide field of view to monitor the whole vessel to minimize number of undetected targets, while narrow width of the detection area should minimize the PA level for blood background. We have demonstrated that high PAFC detection efficiency may be achieved in both cases: using unfocused transducer in OR-PAFC [24,33] or with focused transducer in AR-PAFC. In a prior study, we demonstrated that *in vivo* PAFC can detect CBCs triggered by melanoma and microsurgical invasion. Using an unfocused ultrasound transducer and focused laser beam (i.e., OR-PAFC mode) we were able to detect CBCs only in small (30-50 µm) peripheral blood vessels at depth of 100-150 µm in a mouse ear [24]. The OR-PAFC mode did not provide detection of the same targets circulating in deeper vessels because of the influence of strong optical scattering effect and strong absorption background.

In this work, we applied AR-PAFC mode with the focused ultrasonic transducers for detection of CBCs in relatively deep (up to 5-6 mm) and large (up to 2 mm) vessels in rat and rabbit models. Compared to OR-PAFC, this represents a 36-fold increase in the penetration depth (5.5 mm vs 0.15 mm in average) and 40-fold in the vessel diameter (2 mm vs 0.05 mm in average). Similar observation was made using the AR photoacoustic microscopy [36–38]. Indeed, in case of OR-PAFC only the superficial vessels can be assessed because the spatial resolution is determined by the optical parameters, in particular, by the minimal width of a focused laser beam profile. Due to light scattering in tissue, the highest OR at level of 10 µm could be achieved only for the superficial vessels (30-70 µm in diameter) laying at the shallow depths (0.1-0.15 mm only). Therefore, monitoring of the small superficial blood vessels at good optical conditions (i.e., at low light attenuation due to tissue absorption) provides the highest PAFC sensitivity *in vivo* with the highest PA signal amplitude at a low laser energy requirement. In contrast to these conditions, the scattering and absorption of laser light in deep vessels leads to light intensity attenuation and beam blurring, which reduces the optical resolution. Nevertheless, laser energy is still enough to generate well-detectable PA signals from strongly absorbing objects like RBCs. In these conditions, AR-PAFC platforms have to be applied when the resolution is determined by acoustic parameters of the focused ultrasonic transducer (e.g. at level of 45-80 µm at transducer's frequency of 30-60 MHz). Moreover, combining two PAFC modes (OR-PAFC and AR-PAFC) is definitely possible to make application of PAFC more universal for vessels with different sizes and depths.

PAFC application in humans has to account for the vessel anatomy, thickness of the skin and various properties of tissue layers. For example, vessels with a size of at least 1 mm are usually located at depth of 0.9-1.3 mm at which the influence of light attenuation and scattering becomes notable [32]. Thus, AR-PAFC mode is required because ultrasound waves have lower attenuation and scattering compared to light. In a prior study, we demonstrated that blood background at this wavelength is only slightly higher than at 800-900 nm, however, better depth penetration of 1064 nm makes detection of large circulating targets (e.g., CBCs) in deep large vessels possible.

This PAFC platform can also be used to understand the link between CBCs and CTCs during the progression of cancer and thrombosis [28,34]. Our future goal is to optimize the noninvasive PAFC diagnostic platform for in vivo label-free, real-time detection of cancer-induced CBCs in the bloodstream of melanoma patients.

In general, the PAFC platform can combine detection of CTCs with an analysis of CBCs, allowing for detection of clots before they have a clinical manifestation. This enables identifying patients at increased risk for TE complications which, in turn, could potentially prevent disease progression or recurrence after treatment. Additionally, the real-time monitoring of response to CBCs-therapy may allow an individualized treatment strategy.

Biomedical Optics EXPRESS

Thus, early monitoring of the growth in size and number of small CBCs may predict PE or stroke and prevent it by timely application of therapy.

## 5. Conclusion

In this work we have demonstrated the high potential of *in vivo* PAFC using a fiber-based PA probe with the focused transducer for detection of CBCs of different origins in superficial and deep vessels. This technique definitely provides an increase in sensitivity that is in part due to its ability to monitor nearly the entire blood volume in the body.

## Funding

RF Government grant Nº 14.Z50.31.0044, the National Institute of Health grants R01CA131164 and R01EB017217, CytoAstra LLC, by the National Science Foundation grants OIA 1457888 and DBI 1556068. MAJ was partly supported by the Deutsche Forschungsgemeinschaft (German Research Foundation Grant, JU 2814/1-1).

## Acknowledgments

We thank I. Pelivanov (Univ. of Washington) for providing the customized focused ultrasound transducers and S. Bather (University Hospital Frankfurt) for attentive editing of the manuscript.

## Disclosures

The authors declare that there are no conflicts of interest related to this article.

## References

1. A. Deng, T. Galanis, and M. G. Graham, "Venous thromboembolism in cancer patients," Hosp Pract (1995) **42**(5), 24–33 (2014).
2. R. A. Auer, A. S. Scheer, J. I. McSparron, A. R. Schulman, S. Tuorto, S. Doucette, J. Gonsalves, and Y. Fong, "Postoperative venous thromboembolism predicts survival in cancer patients," Ann. Surg. **255**(5), 963–970 (2012).
3. D. Farge, P. Debourdeau, M. Beckers, C. Baglin, R. M. Bauersachs, B. Brenner, D. Brilhante, A. Falanga, G. T. Gerotzafias, N. Haim, A. K. Kakkar, A. A. Khorana, R. Lecumberri, M. Mandala, M. Marty, M. Monreal, S. A. Mousa, S. Noble, I. Pabinger, P. Prandoni, M. H. Prins, M. H. Qari, M. B. Streiff, K. Syrigos, H. Bounameaux, and H. R. Büller, "International clinical practice guidelines for the treatment and prophylaxis of venous thromboembolism in patients with cancer," J. Thromb. Haemost. **11**(1), 56–70 (2013).
4. C. Tymvios, S. Jones, C. Moore, S. C. Pitchford, C. P. Page, and M. Emerson, "Real-time measurement of non-lethal platelet thromboembolic responses in the anaesthetized mouse," Thromb. Haemost. **99**(2), 435–440 (2008).
5. E. I. Galanzha, M. Sarimollaoglu, D. A. Nedosekin, S. G. Keyrouz, J. L. Mehta, and V. P. Zharov, "In vivo flow cytometry of circulating clots using negative photothermal and photoacoustic contrasts," Cytometry A **79A**(10), 814–824 (2011).
6. L. Frank, C. Lebreton-Decoster, G. Godeau, B. Coulomb, and J. Jozefonvicz, "Dextran derivatives modulate collagen matrix organization in dermal equivalent," J. Biomater. Sci. Polym. Ed. **17**(5), 499–517 (2006).
7. V. L. Feigin, C. M. Lawes, D. A. Bennett, S. L. Barker-Collo, and V. Parag, "Worldwide stroke incidence and early case fatality reported in 56 population-based studies: a systematic review," Lancet Neurol. **8**(4), 355–369 (2009).
8. D. K. Dressler, "Death by clot: acute coronary syndromes, ischemic stroke, pulmonary embolism, and disseminated intravascular coagulation," AACN Adv. Crit. Care **20**(2), 166–176 (2009).
9. W. Ageno, C. Becattini, T. Brighton, R. Selby, and P. W. Kamphuisen, "Cardiovascular risk factors and venous thromboembolism: a meta-analysis," Circulation **117**(1), 93–102 (2008).
10. F. A. Anderson, Jr., H. B. Wheeler, R. J. Goldberg, D. W. Hosmer, N. A. Patwardhan, B. Jovanovic, A. Forcier, and J. E. Dalen, "A population-based perspective of the hospital incidence and case-fatality rates of deep vein thrombosis and pulmonary embolism. The Worcester DVT Study," Arch. Intern. Med. **151**(5), 933–938 (1991).
11. J. A. Heit, W. M. O'Fallon, T. M. Petterson, C. M. Lohse, M. D. Silverstein, D. N. Mohr, and L. J. Melton 3rd, "Relative impact of risk factors for deep vein thrombosis and pulmonary embolism: a population-based study," Arch. Intern. Med. **162**(11), 1245–1248 (2002).
12. R. Gerrah and O. David, "In vivo quantification of clot formation in extracorporeal circuits," Stud. Health Technol. Inform. **184**, 148–150 (2013).
13. A. A. Khorana, "Cancer-associated thrombosis: updates and controversies," Hematology (Am. Soc. Hematol. Educ. Program) **2012**, 626–630 (2012).

Biomedical Optics EXPRESS


14. R. H. White, H. Zhou, and P. S. Romano, "Incidence of symptomatic venous thromboembolism after different elective or urgent surgical procedures," Thromb. Haemost. **90**(3), 446–455 (2003).
15. J. G. Geng, "Interaction of vascular endothelial cells with leukocytes, platelets and cancer cells in inflammation, thrombosis and cancer growth and metastasis," Acta Pharmacol. Sin. **24**(12), 1297–1300 (2003).
16. P. Jurasz, D. Alonso-Escolano, and M. W. Radomski, "Platelet--cancer interactions: mechanisms and pharmacology of tumour cell-induced platelet aggregation," Br. J. Pharmacol. **143**(7), 819–826 (2004).
17. T. Tsuruo, "Platelet aggregation in the formation of tumor metastasis," Proc. of the Japan Academy **84**, 189–198 (2008).
18. G. W. Tormoen, K. M. Haley, R. L. Levine, and O. J. T. McCarty, "Do circulating tumor cells play a role in coagulation and thrombosis?" Front. Oncol. **2**, 115 (2012).
19. J. C. Grotta and A. V. Alexandrov, "Preventing stroke: is preventing microemboli enough?" Circulation **103**(19), 2321–2322 (2001).
20. J. D. Marsh and S. G. Keyrouz, "Stroke prevention and treatment," J. Am. Coll. Cardiol. **56**(9), 683–691 (2010).
21. A. Blum, A. Bellou, F. Guillemin, P. Douek, M. C. Laprévote-Heully, D. Wahl, and GENEPI study group, "Performance of magnetic resonance angiography in suspected acute pulmonary embolism," Thromb. Haemost. **93**(3), 503–511 (2005).
22. Y. Yang, D. G. Grosset, Q. Li, A. Shuaib, and K. R. Lees, "Turbulence and circulating cerebral emboli detectable at Doppler ultrasonography: a differentiation study in a stenotic middle cerebral artery model," AJNR Am. J. Neuroradiol. **23**(7), 1229–1236 (2002).
23. S. Falati, P. Gross, G. Merrill-Skoloff, B. C. Furie, and B. Furie, "Real-time in vivo imaging of platelets, tissue factor and fibrin during arterial thrombus formation in the mouse," Nat. Med. **8**(10), 1175–1180 (2002).
24. M. A. Juratli, Y. A. Menyaev, M. Sarimollaoglu, E. R. Siegel, D. A. Nedosekin, J. Y. Suen, A. V. Melerzanov, T. A. Juratli, E. I. Galanzha, and V. P. Zharov, "Real-time label-free embolus detection using in vivo photoacoustic flow cytometry," PLoS One **11**(5), e0156269 (2016).
25. E. I. Galanzha, M. G. Viegas, T. I. Malinsky, A. V. Melerzanov, M. A. Juratli, M. Sarimollaoglu, D. A. Nedosekin, and V. P. Zharov, "In vivo acoustic and photoacoustic focusing of circulating cells," Sci. Rep. **6**(1), 21531 (2016).
26. Y. A. Menyaev, D. A. Nedosekin, M. Sarimollaoglu, M. A. Juratli, E. I. Galanzha, V. V. Tuchin, and V. P. Zharov, "Optical clearing in photoacoustic flow cytometry," Biomed. Opt. Express **4**(12), 3030–3041 (2013).
27. D. A. Nedosekin, M. A. Juratli, M. Sarimollaoglu, C. L. Moore, N. J. Rusch, M. S. Smeltzer, V. P. Zharov, and E. I. Galanzha, "Photoacoustic and photothermal detection of circulating tumor cells, bacteria and nanoparticles in cerebrospinal fluid in vivo and ex vivo," J. Biophotonics **6**(6-7), 523–533 (2013).
28. M. A. Juratli, D. A. Nedosekin, M. Sarimollaoglu, E. R. Siegel, E. I. Galanzha, and V. P. Zharov, "Circulating tumor cells as predictive marker in metastatic disease," in *Perioperative Inflammation as Triggering Origin of Metastasis Development* (Springer, 2017), pp. 109–122.
29. M. A. Juratli, E. R. Siegel, D. A. Nedosekin, M. Sarimollaoglu, A. Jamshidi-Parsian, C. Cai, Y. A. Menyaev, J. Y. Suen, E. I. Galanzha, and V. P. Zharov, "In vivo long-term monitoring of circulating tumor cells fluctuation during medical interventions," PLoS One **10**(9), e0137613 (2015).
30. N. A. Koonce, M. A. Juratli, C. Cai, M. Sarimollaoglu, Y. A. Menyaev, J. Dent, C. M. Quick, R. P. M. Dings, D. Nedosekin, V. Zharov, and R. J. Griffin, "Real-time monitoring of circulating tumor cell (CTC) release after nanodrug or tumor radiotherapy using in vivo flow cytometry," Biochem. Biophys. Res. Commun. **492**(3), 507–512 (2017).
31. M. A. Juratli, M. Sarimollaoglu, D. A. Nedosekin, A. V. Melerzanov, V. P. Zharov, and E. I. Galanzha, "Dynamic fluctuation of circulating tumor cells during cancer progression," Cancers (Basel) **6**(1), 128–142 (2014).
32. Y. A. Menyaev, K. A. Carey, D. A. Nedosekin, M. Sarimollaoglu, E. I. Galanzha, J. S. Stumhofer, and V. P. Zharov, "Preclinical photoacoustic models: application for ultrasensitive single cell malaria diagnosis in large vein and artery," Biomed. Opt. Express **7**(9), 3643–3658 (2016).
33. M. A. Juratli, M. Sarimollaoglu, E. R. Siegel, D. A. Nedosekin, E. I. Galanzha, J. Y. Suen, and V. P. Zharov, "Real-time monitoring of circulating tumor cell release during tumor manipulation using in vivo photoacoustic and fluorescent flow cytometry," Head Neck **36**(8), 1207–1215 (2014).
34. E. I. Galanzha and V. P. Zharov, "Photoacoustic flow cytometry," Methods **57**(3), 280–296 (2012).
35. H. J. Jawad, M. Sarimollaoglu, A. S. Biris, and V. P. Zharov, "Dynamic blood flow phantom with negative and positive photoacoustic contrasts," Biomed. Opt. Express **9**(10), 4702–4713 (2018).
36. W. Xing, L. Wang, K. Maslov, and L. V. Wang, "Integrated optical- and acoustic-resolution photoacoustic microscopy based on an optical fiber bundle," Opt. Lett. **38**(1), 52–54 (2013).
37. S. Park, C. Lee, J. Kim, and C. Kim, "Acoustic resolution photoacoustic microscopy," Biomed. Eng. Lett. **4**(3), 213–222 (2014).
38. M. Moothanchery and M. Pramanik, "Performance characterization of a switchable acoustic resolution and optical resolution photoacoustic microscopy system," Sensors (Basel) **17**(2), 357 (2017).